LETTER

doi:10.1038/nature14001

Predicting immunogenic tumour mutations by combining mass spectrometry and exome sequencing

Mahesh Yadav[1]*, Suchit Jhunjhunwala[1]*, Qui T. Phung[1], Patrick Lupardus[1], Joshua Tanguay[1], Stephanie Bumbaca[1], Christian Franci[1], Tommy K. Cheung[1], Jens Fritsche[2], Toni Weinschenk[2], Zora Modrusan[1], Ira Mellman[1], Jennie R. Lill[1]§ & Lélia Delamarre[1]§

Human tumours typically harbour a remarkable number of somatic mutations[1]. If presented on major histocompatibility complex class I molecules (MHCI), peptides containing these mutations could potentially be immunogenic as they should be recognized as 'non-self' neo-antigens by the adaptive immune system. Recent work has confirmed that mutant peptides can serve as T-cell epitopes[2–9]. However, few mutant epitopes have been described because their discovery required the laborious screening of patient tumour-infiltrating lymphocytes for their ability to recognize antigen libraries constructed following tumour exome sequencing. We sought to simplify the discovery of immunogenic mutant peptides by characterizing their general properties. We developed an approach that combines whole-exome and transcriptome sequencing analysis with mass spectrometry to identify neo-epitopes in two widely used murine tumour models. Of the >1,300 amino acid changes identified, ~13% were predicted to bind MHCI, a small fraction of which were confirmed by mass spectrometry. The peptides were then structurally modelled bound to MHCI. Mutations that were solvent-exposed and therefore accessible to T-cell antigen receptors were predicted to be immunogenic. Vaccination of mice confirmed the approach, with each predicted immunogenic peptide yielding therapeutically active T-cell responses. The predictions also enabled the generation of peptide–MHCI dextramers that could be used to monitor the kinetics and distribution of the anti-tumour T-cell response before and after vaccination. These findings indicate that a suitable prediction algorithm may provide an approach for the pharmacodynamic monitoring of T-cell responses as well as for the development of personalized vaccines in cancer patients.

Although CD8 T cells can recognize tumour cells and mediate tumour regression following immunotherapy[10], the antigens driving effective anti-tumour CD8 T-cell responses remain largely unknown. Tumour antigens can be classified into two categories: tumour-associated self-antigens (for example, cancer-testis antigens, differentiation antigens) and antigens derived from tumour-specific mutant proteins. Since the presentation of self-antigens in the thymus may result in the elimination of high-avidity T cells, mutant neo-antigens seem likely to be more immunogenic. However, identifying these antigens has proved problematic, having evaded identification by mass spectrometry, which typically relies on sequence elucidation using public proteomic databases that do not contain patient-specific mutations. Conversely, relying on transcriptomic or exome-sequence analysis for mutation identification followed by MHCI binding prediction algorithms typically yields too many candidate mutant peptides to be easily evaluated. The strength of our approach lies in combining these two powerful and well-established analytical tools to identify tumour-associated mutated peptides that are presented on MHCI (Fig. 1a).

We performed whole-exome sequencing on MC-38 and TRAMP-C1 mouse tumour cell lines to identify tumour-specific point mutations. Coding variants were called relative to the reference mouse genome to identify 4,285 and 949 non-synonymous variants in MC-38 and TRAMP-C1, respectively (Fig. 1b). To select for high-confidence mutations and focus on the mutations likely to be expressed in the majority of the tumour cells, we subsequently selected RNA-seq-based variants that were present at a minimum of 20% allelic frequency and overlapped with the exome-based variants. This resulted in 1,290 and 67 expressed mutations in MC-38 and TRAMP-C1, respectively. Next we identified 170 predicted neo-epitopes in MC-38 and 6 predicted neo-epitopes in TRAMP-C1 using the NETMHC-3.4 algorithm[11] (Fig. 1b, Supplementary Tables 1 and 2). Despite high density exome reads, only a small number of non-synonymous variants and predicted neo-epitopes in TRAMP-C1 were identified. This low mutational frequency may at least partially explain the low immunogenicity of TRAMP-C1 observed *in vivo* (that is, paucity of tumour-infiltrating lymphocytes (TILs)), compared to MC-38 tumours (Extended Data Fig. 1a).

Next, we conducted mass spectrometric analysis for MHCI-presented peptides and searched against the transcriptome-generated FASTA database (Fig. 1a). This revealed 2,332 unique H-2K^b epitopes and 3,907 unique H-2D^b epitopes presented in MC-38, and 1,651 unique H-2K^b epitopes and 1,980 unique H-2D^b epitopes presented in TRAMP-C1 cells (Supplementary Table 3). The reduced number of epitopes identified for TRAMP-C1 compared to MC-38 probably reflects weaker MHCI surface expression on TRAMP-C1 cells[12] (Extended Data Fig. 1b). Overall we observed that peptides derived from abundant transcripts are more likely to be presented by MHCI (Fig. 1c, Supplementary Tables 3 and 4), as observed by others[13,14].

Of the 1,290 and 67 amino acid changes in MC-38 and TRAMP-C1, respectively, only 7 (7 in MC-38 and 0 in TRAMP-C1) were found to be presented on MHCI by mass spectrometry (Table 1) after manual validation and comparison with a synthetically generated version of the peptide for spectral accuracy (Extended Data Fig. 2). All but one of these neo-epitopes were predicted to bind MHCI (half-maximum inhibitory concentration (IC_{50}) < 500 nM, Table 1). Both wild-type and mutant transcripts corresponding to the peptides were expressed by MC-38 cells (Supplementary Table 5 and Extended Data Fig. 3) and although most of the exact counterpart wild-type peptides were also predicted to bind MHCI, only three were detected by mass spectrometry (Extended Data Fig. 4). The mutations were not coded in the germline as the sequence for all 7 genes was confirmed as wild type at the position of interest in the genome of a C57BL/6 mouse. These proteins have no known role in oncogenesis except Med12, which is frequently mutated in prostate cancer and in smooth muscle tumours[15,16].

The small number of mutated peptides identified by mass spectrometry compared to the number of peptides predicted to be presented may be attributed in part to the sensitivity of the peptide purification and mass spectrometric approach, but also suggests that a limiting factor to presentation could be the peptide generation and transport into the endoplasmic reticulum[17]. On the other hand, mass spectrometry allows

[1]Genentech, South San Francisco, California 94080, USA. [2]Immatics Biotechnologies GmbH, 72076 Tubingen, Germany.
*These authors contributed equally to this work.
§These authors jointly supervised this work.

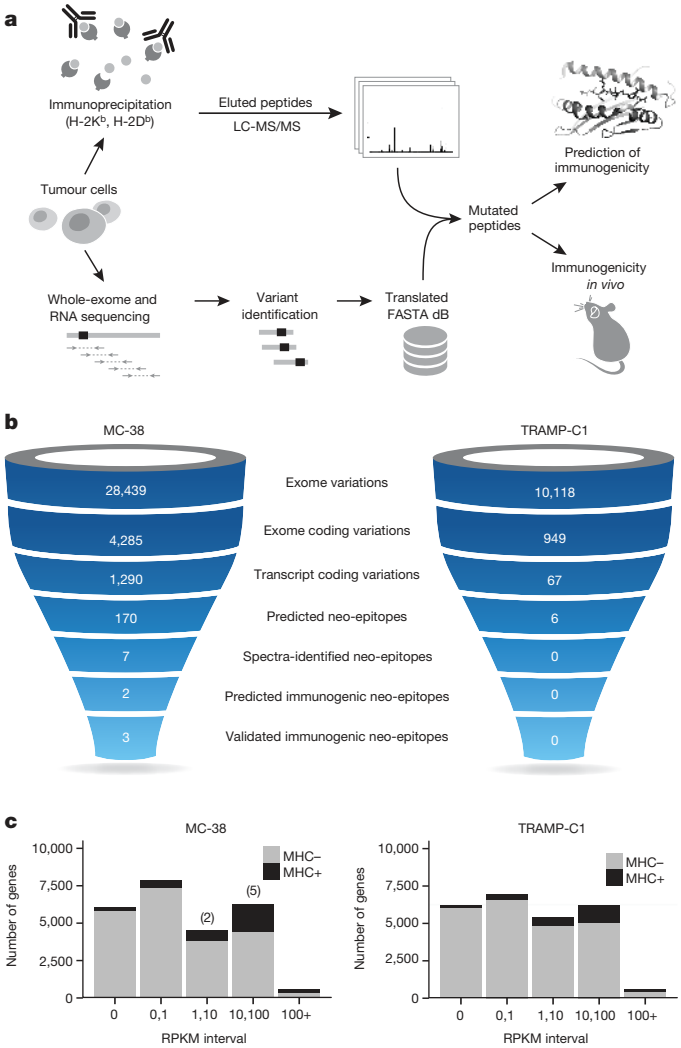

Figure 1 | Identification of MHCI-presented tumour-specific mutations in MC-38 and TRAMP-C1 tumour cell lines. **a**, Schematic of the approach for identifying mutated MHCI-presented peptides using sequencing in combination with mass spectrometry. After immunoprecipitation peptides were analysed using tandem mass spectrometry and were searched against a customized FASTA database based on RNA-seq. Immunogenicity of mutated peptides was further predicted *in silico* and validated using *in vivo* immunogenicity studies. **b**, Flowcharts for the number of genomic variations or variant peptides identified at each stage of analysis, and finally the number of peptides validated as immunogenic. **c**, RNA-seq expression profiles of genes corresponding to MHCI-presented peptides. The *x* axis represents expression levels (categorized into five reads per kilobase per million reads mapped (RPKM) intervals). The numbers of genes for each RPKM category that manifest MHCI-presented peptide(s) are shown (MHC+), as well as the rest of the genes (MHC−). The numbers of mutated MHCI-presented peptides identified by mass spectrometry in each RPKM interval are indicated above the bars.

a stringent filter to be incorporated into the workflow by selecting for peptides with sufficient expression and presentation by MHCI, therefore ensuring only the peptides most likely to yield an immunological response are further investigated.

We next asked if immunogenicity of the identified neo-epitopes could be predicted. Although there is a correlation between peptide binding affinity for MHCI and immunogenicity, other factors also contribute[18]. For example, interaction of the mutated amino acid with the T-cell antigen receptor (TCR) is likely to be essential for the recognition of the mutated peptide as 'foreign'. This is especially true when the counterpart wild-type peptide is also presented on MHCI. Five out of the seven neo-epitopes exhibited high binding affinity prediction (Table 1, $IC_{50} < 50$ nM). The other neo-epitopes exhibited lower binding affinity prediction, suggesting that they might be less immunogenic. We next used published crystal structures of H-2D^b and H-2K^b and a Rosetta-based algorithm[19] to model each of the mutant peptides in complex with MHCI and analyse the potential for the mutant residue in each neo-epitope to interact with the TCR. In general, TCR recognition of displayed peptides is mediated by interactions with peptide residues 3 through 7 (ref. 20). Among the peptides with high binding scores only in the Reps1 and Adpgk peptides did the mutation lie within this range. Structure modelling also predicted that the mutated residues were oriented towards the solvent interface, and were thus judged to have good potential to be immunogenic (Table 1 and Fig. 2)[20]. On the other hand, the mutations in the Irgq, Aatf and Dpagt1 neo-epitopes were found near the carboxy-terminal end of the peptide, which probably falls outside of the TCR binding region and suggests that these neo-epitopes were unlikely to be immunogenic despite the increase in predicted binding affinity to MHCI in comparison to the counterpart wild-type peptide (Table 1 and Fig. 2).

We next evaluated the immunogenicity of mutated tumour antigens *in vivo* by immunizing C57BL/6 mice with peptides encoding the mutated epitopes in combination with adjuvant and measured CD8 T-cell responses using peptide–MHCI dextramers. Three out of six peptides elicited CD8 T-cell responses (Fig. 3a). We had predicted Reps1 and Adpgk to be immunogenic on the basis of structure and binding affinity prediction, and both elicited strong CD8 T-cell responses. Of the four peptides predicted to be non-immunogenic, only Dpagt1 induced a weak CD8 T-cell response. The exact counterpart wild-type peptides of Reps1 and Adpgk were not immunogenic (Extended Data Fig. 5a–d).

We confirmed the immunogenicity of these mutated peptides in the context of the MC-38 tumours grown in C57BL/6 mice by analysing TILs and staining with peptide–MHCI dextramers. We found that CD8 T cells specific for Reps1, Adpgk and Dpagt1 were enriched in the tumour bed (Fig. 3b) but not T cells specific for the other mutant peptides (data not shown). Although there was heterogeneity, Adpgk-specific CD8 T cells were the most abundant of the three, and this was specific to MC-38 tumours as no Adpgk-specific CD8 T cells were detected in TRAMP-C1 tumours (Extended Data Fig. 5e). These results show that CD8 T-cell responses are generated against neo-epitopes in MC-38 tumours and further supports our hypothesis that structural correlation predicting solvent exposure of the mutation combined with MHCI-binding affinity may provide suitable criteria for triaging potential

Table 1 | Summary of mutant peptides presented by MHCI in the MC-38 cell line

Gene	Peptide	MHC allele	IC_{50} (mut)	IC_{50} (WT)	Mutation position	Immunogenicity prediction
Dpagt1	SIIVFNL[V/**L**]	*H-2K*^{b}	8	34	Anchor (P8)	–
Reps1	AQL[P/**A**]NDVVL	*H-2D*^{b}	9	100	Solvent (P4)	+
Adpgk	ASMTN[R/**M**]ELM	*H-2D*^{b}	2	3	Solvent (P6)	+
Cpne1	SSP[D/**Y**]SLHYL	*H-2D*^{b}	211	685	Solvent (P4)	–
Irgq	AALLNSA[G/**V**]L	*H-2D*^{b}	3	52	Solvent (P8)	–
Aatf	MAPIDHT[A/**T**]M	*H-2D*^{b}	30	102	Solvent (P8)	–
Med12	DPSSSVLFE[D/**Y**]	*H-2K*^{b}	38,300	39,411	No structure	–

The IC_{50} values (IC_{50} predicted by NetMHC-3.4 in nM units) are shown. Peptides with $IC_{50} < 500$ nM are predicted to bind MHCI. The mutant amino acid's position is described (whether it was anchored to a MHC molecule or solvent-exposed), based on homology to known MHC–peptide complex structures. The immunogenicity prediction is simply based on $IC_{50} < 50$ nM for the peptide, and position (P3–7: which are likely to interact with TCR) and solvent exposure of the mutation. Mutation is indicated in bold next to the wild-type amino acid in the bracket in the peptide sequences.

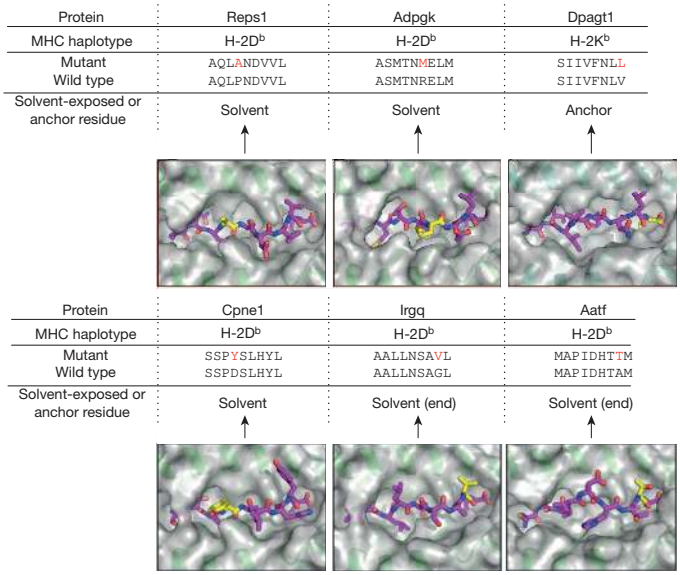

Figure 2 | Modelling of mutant peptide–MHCI complexes. Mutant peptides were modelled into peptide–MHCI structures using existing crystal structures from the Protein Data Bank as starting models and optimizing the conformation of the bound mutant peptide using the program FlexPepDock[19]. H-2D^b and H-2K^b MHC haplotypes are shown in green. Modelled peptides are shown in magenta as stick models, with the mutated residue highlighted in yellow.

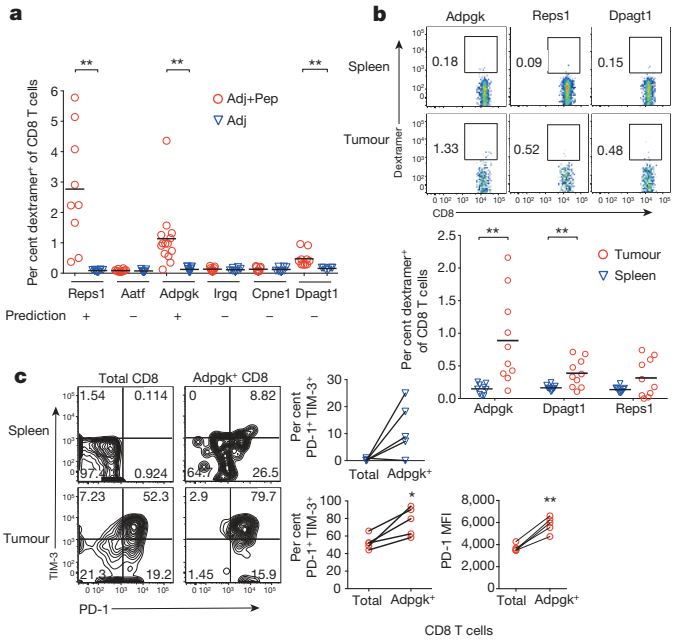

Figure 3 | Immunogenicity of mutated peptides *in vivo*. **a**, C57BL/6 mice were immunized with adjuvant (anti-CD40 antibody plus poly(I:C)) alone (Adj) or in combination with a mix of all long mutated peptides from Table 1 (50 μg each) (Adj+Pep). Med12 peptide was not included because it was not predicted to bind to MHCI. After two immunizations on day 0 and day 14, spleens were collected at day 21 and CD8 T cells were stained with different phycoerythrin (PE)-labelled peptide–MHCI dextramers (indicated on *x* axis) and analysed by flow cytometry. The adjuvant alone (Adj) group is used as the reference for immunogenicity. Each dot represents individual mouse with bar representing mean. Pooled data from two independent experiments are shown with $n \geq 6$ (Adj) or $n \geq 9$ (Adj+Pep) mice per group. **b**, Frequency of Adpgk, Reps1 or Dpagt1–MHCI-specific CD8 T cells among total CD8 T cells in MC-38 tumour-bearing mice (tumour size ~500 mm^3). The graph on the bottom represents pooled tumour data from ten individual mice. The bars represent mean, $^{**}P \leq 0.01$ (two-tailed unpaired *t*-test). **c**, PD-1 and TIM-3 surface expression was measured on Adpgk–H-2D^b dextramer$^+$ or total CD8 T cells from panel **b**. A representative staining from spleen (top) and tumour (bottom) is shown with the graph on right showing pooled data from five mice. For tumours, PD-1 median intensity of fluorescence (MFI) (gated on PD-1$^+$ cells) in the indicated population is also shown. $^*P \leq 0.05$, $^{**}P \leq 0.01$ (two-tailed paired *t*-test).

immunogenic peptides. Further analysis of a larger peptide data set will give a better indication of the statistical utility of this method.

Bulk TILs are usually analysed to monitor frequency and the phenotype of anti-tumour CD8 T-cell responses, which may not provide a true assessment because only a fraction of CD8 TILs are tumour-specific[6]. Using peptide–MHCI dextramers for the three immunogenic peptides, we were able to compare the anti-tumour TILs with the bulk TILs in MC-38 tumours. Although the frequency of tumour-specific CD8 T cells infiltrating tumours appear to increase initially, we could not discern a clear correlation between infiltration and tumour growth (Extended Data Fig. 6). Interestingly, a vast majority (76.9 ± 7.1% s.e.m.) of tumour-specific CD8 TILs, detected using Adpgk–H-2D^b dextramer, co-expressed PD-1 and TIM-3, compared to bulk CD8 TILs (52.6 ± 3.6%) (Fig. 3c). PD-1 and TIM-3 are inhibitory receptors expressed upon T cell activation and their coexpression on CD8 T cells is associated with chronic antigen stimulation leading to T cell exhaustion[21–23]. We also observed a population of CD8 TILs (Adpgk–H-2D^b dextramer-negative) that expressed PD-1 and TIM-3. This could be due to the effect of the tumour microenvironment on CD8 T cells irrespective of their specificity[24–26]. However, the expression of PD-1 on bulk CD8 TILs was lower than tumour Adpgk-specific CD8 T cells (PD-1 MFI (median fluorescence intensity), Fig. 3c). These results highlight the differential phenotypic characteristics of tumour-reactive cells in the tumour microenvironment and suggest that tumour-specific CD8 T cells exhibit a more exhausted state, in line with recent observations in human tumours[6].

To determine if CD8 T cells induced against neo-epitopes could provide protective anti-tumour immunity, healthy mice were immunized with the mutated peptides (Adpgk, Reps1 and Dpagt1) and subsequently challenged with MC-38 tumour cells (Fig. 4a). Tumour growth was completely inhibited in most of the animals in the vaccine group compared to adjuvant alone (Fig. 4b). Two of the animals that had substantial tumour growth in the vaccine group also had the lowest frequency of Adpgk-reactive CD8 T cells in blood before tumour inoculation (Fig. 4c and Extended Data Fig. 7), strongly supporting that CD8 T-cell responses specific to mutated peptides conferred protection.

Next, we asked if the neo-epitope-specific CD8 T-cell responses could be further amplified in tumour-bearing mice upon immunization (Fig. 4d). After a single immunization, the frequency of Adpgk-reactive CD8 T cells increased remarkably in the spleen of tumour-bearing mice compared to immunized non-tumour-bearing animals (Fig. 4e). Interestingly, we did not observe a similar enhancement of the CD8 T-cell response against Reps1 and Dpagt1 (Extended Data Fig. 8), suggesting that Adpgk is the immuno-dominant neo-epitope in tumour-bearing mice. We also observed a nearly threefold increase in accumulation of Adpgk-reactive CD8 T cells among total CD8 TILs in the tumours (Fig. 4e). Peptide vaccination also increased overall infiltration of CD45$^+$ cells and CD8$^+$ T cells in tumours, which resulted into nearly 20-fold increase in the frequency of neo-epitope-specific CD8 T cells among the total live cells in the tumour (Fig. 4f and Extended Data Fig. 9a).

We next analysed the phenotype of peptide-specific CD8 T cells induced by peptide vaccination. We found that the frequency of PD-1 and TIM-3 expressing Adpgk-specific CD8 TILs was reduced after vaccination, and the surface expression of PD-1 and TIM-3 on these cells was also reduced (Fig. 4g, h). This might be an adjuvant effect as it was also seen in the adjuvant alone group. These results suggest that tumour-specific T cells exhibit a less exhausted phenotype after vaccination, and this was further confirmed by the higher percentage of IFN-γ-expressing CD8 and CD4 TILs in the tumours from vaccinated mice (Fig. 4i and Extended Data Fig. 9b).

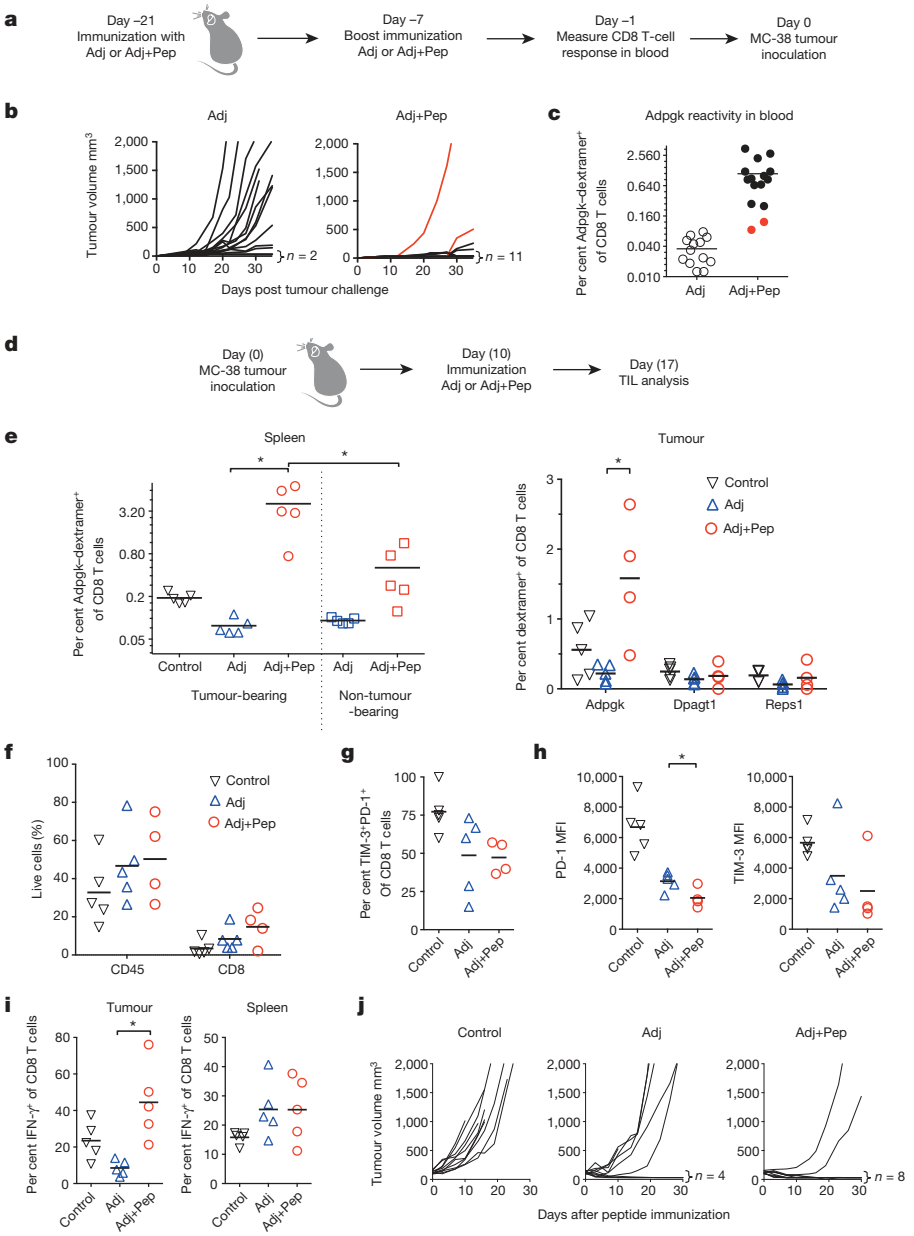

Figure 4 | Vaccination with immunogenic peptides provides protection and delays tumour growth. **a**–**c**, C57BL/6 mice were immunized with mutated peptides (Adpgk, Reps1 and Dpagt1, 50 μg each) and anti-CD40 antibody plus poly(I:C) as adjuvant (Adj+Pep) or adjuvant alone (Adj) followed by inoculation with MC-38 tumour cells as outlined in **a**. **b**, Tumour growth for Adj ($n = 14$) or Adj+Pep ($n = 15$) groups. Two mice in the Adj+Pep group that showed tumour growth are shown in red. **c**, Frequency of CD8 T cells in blood (at day −1) stained with Adpgk–H-2D^b dextramer and analysed by flow cytometry. The red dots in the graph correspond to the mice that developed tumours in the Adj+Pep group (in **b**). Pooled data from two independent experiments are shown. **d**–**j**, C57BL/6 mice were inoculated with MC-38 tumour cells, and 10 days later immunized with mutated peptides (Adpgk, Reps1 and Dpagt1, 50 μg each) with adjuvant (Adj+Pep), adjuvant alone (Adj) or left untreated (control) as outlined in **d**. **e**, Seven days post immunization, spleen or tumour cells were stained with PE-labelled peptide–MHCI dextramers for the indicated peptide (for tumours) or with Adpgk–H-2D^b dextramer (for spleen) and analysed by flow cytometry. For comparison, non-tumour-bearing mice were also immunized with adjuvant alone (Adj) or adjuvant with peptides (Adj+Pep) and splenic CD8 T cells were stained with PE-labelled Adpgk–H-2D^b dextramer at day 7. **f**, CD45$^+$ or CD8$^+$ T cells in tumours shown as percentage of total live cell gate. **g**, **h**, Frequency of TIM-3$^+$PD-1$^+$ cells and mean intensity of fluorescence (MFI) of PD-1 (on PD-1$^+$) and TIM-3 (on PD-1$^+$TIM-3$^+$) among Adpgk–H-2D^b dextramer$^+$ CD8 TILs measured by flow cytometry. **i**, TILs or splenocytes were stimulated with PMA and ionomycin and IFN-γ production in CD8 T cells was determined by intracellular cytokine staining and analysis by flow cytometry. **j**, Tumour growth in control, Adj or Adj+Pep groups ($n = 10$ each group). **e**–**j**, Data are representative of two independent experiments. The bars represent mean. *$P \leq 0.05$ (two-tailed unpaired t-test).

Finally, even in this more difficult therapeutic setting, tumour-bearing mice vaccinated with mutated peptides showed remarkable and sustainable inhibition of tumour growth compared to untreated control or adjuvant alone groups (Fig. 4j). Thus, simple peptide vaccination with the predicted neo-epitopes generated sufficient T-cell immunity to reject a previously established tumour.

The identification of epitopes that drive the immune response in cancer is essential to the understanding and manipulation of CD8 T-cell immune responses for clinical benefit. Recent studies in mice and humans have suggested that tumour-specific mutations probably have a key role in shaping the anti-tumour response; however, their identification has remained a challenge[2–9]. We developed a novel strategy to identify neo-epitopes by combining whole-exome/transcriptome sequencing and mass spectrometry analysis, along with a structural prediction algorithm to predict MHCI peptide immunogenicity. This will not only facilitate generation of novel vaccines but also make it feasible to track tumour-specific T cells, which could be invaluable for prognosis of cancer patients in this era of cancer immunotherapy.

To be fully useful in the clinic, it will probably be necessary to simplify the approach further, so as to rely entirely on computational predictions of peptide binding rather than mass spectrometry. A purely computational approach, including a MHCI-haplotype-specific structural prediction, would require only whole-exome/transcriptome sequencing of a patient's tumour, which is beginning to be routinely determined.

Online Content Methods, along with any additional Extended Data display items and Source Data, are available in the online version of the paper; references unique to these sections appear only in the online paper.

Received 27 May; accepted 28 October 2014.

1. Lawrence, M. S. *et al.* Mutational heterogeneity in cancer and the search for new cancer-associated genes. *Nature* **499,** 214–218 (2013).
2. Matsushita, H. *et al.* Cancer exome analysis reveals a T-cell-dependent mechanism of cancer immunoediting. *Nature* **482,** 400–404 (2012).
3. DuPage, M., Mazumdar, C., Schmidt, L. M., Cheung, A. F. & Jacks, T. Expression of tumour-specific antigens underlies cancer immunoediting. *Nature* **482,** 405–409 (2012).
4. Castle, J. C. *et al.* Exploiting the mutanome for tumor vaccination. *Cancer Res.* **72,** 1081–1091 (2012).
5. van Rooij, N. *et al.* Tumor exome analysis reveals neoantigen-specific T-cell reactivity in an ipilimumab-responsive melanoma. *J. Clin. Oncol.* **31,** e439–e442 (2013).
6. Gros, A. *et al.* PD-1 identifies the patient-specific CD8+ tumor-reactive repertoire infiltrating human tumors. *J. Clin. Invest.* **124,** 2246–2259 (2014).

7. Tran, E. *et al.* Cancer immunotherapy based on mutation-specific CD4+ T cells in a patient with epithelial cancer. *Science* **344,** 641–645 (2014).
8. Wick, D. A. *et al.* Surveillance of the tumor mutanome by T cells during progression from primary to recurrent ovarian cancer. *Clin. Cancer Res.* **20,** 1125–1134 (2014).
9. Brown, S. D. *et al.* Neo-antigens predicted by tumor genome meta-analysis correlate with increased patient survival. *Genome Res.* **24,** 743–750 (2014).
10. Chen, D. S. & Mellman, I. Oncology meets immunology: the cancer-immunity cycle. *Immunity* **39,** 1–10 (2013).
11. Lundegaard, C. *et al.* NetMHC-3.0: accurate web accessible predictions of human, mouse and monkey MHC class I affinities for peptides of length 8–11. *Nucleic Acids Res.* **36,** W509–W512 (2008).
12. Gujar, S. A., Pan, D. A., Marcato, P., Garant, K. A. & Lee, P. W. Oncolytic virus-initiated protective immunity against prostate cancer. *Mol. Ther.* **19,** 797–804 (2011).
13. Fortier, M. H. *et al.* The MHC class I peptide repertoire is molded by the transcriptome. *J. Exp. Med.* **205,** 595–610 (2008).
14. Granados, D. P. *et al.* MHC I-associated peptides preferentially derive from transcripts bearing miRNA response elements. *Blood* **119,** e181–e191 (2012).
15. Barbieri, C. E. *et al.* Exome sequencing identifies recurrent SPOP, FOXA1 and MED12 mutations in prostate cancer. *Nature Genet.* **44,** 685–689 (2012).
16. Bertsch, E. *et al.* MED12 and HMGA2 mutations: two independent genetic events in uterine leiomyoma and leiomyosarcoma. *Mod. Pathol.* **27,** 1144–1153 (2014).
17. Goldberg, A. L. Functions of the proteasome: from protein degradation and immune surveillance to cancer therapy. *Biochem. Soc. Trans.* **35,** 12–17 (2007).
18. Sette, A. *et al.* The relationship between class I binding affinity and immunogenicity of potential cytotoxic T cell epitopes. *J. Immunol.* **153,** 5586–5592 (1994).
19. London, N., Raveh, B., Cohen, E., Fathi, G. & Schueler-Furman, O. Rosetta FlexPepDock web server–high resolution modeling of peptide-protein interactions. *Nucleic Acids Res.* **39,** W249–W253 (2011).
20. Rudolph, M. G., Stanfield, R. L. & Wilson, I. A. How TCRs bind MHCs, peptides, and coreceptors. *Annu. Rev. Immunol.* **24,** 419–466 (2006).
21. Jin, H. T. *et al.* Cooperation of Tim-3 and PD-1 in CD8 T-cell exhaustion during chronic viral infection. *Proc. Natl Acad. Sci. USA* **107,** 14733–14738 (2010).
22. Jin, H. T., Ahmed, R. & Okazaki, T. Role of PD-1 in regulating T-cell immunity. *Curr. Top. Microbiol. Immunol.* **350,** 17–37 (2011).
23. Wherry, E. J. T cell exhaustion. *Nature Immunol.* **12,** 492–499 (2011).
24. Fourcade, J. *et al.* Upregulation of Tim-3 and PD-1 expression is associated with tumor antigen-specific CD8+ T cell dysfunction in melanoma patients. *J. Exp. Med.* **207,** 2175–2186 (2010).
25. Fourcade, J. *et al.* $CD8^+$ T cells specific for tumor antigens can be rendered dysfunctional by the tumor microenvironment through upregulation of the inhibitory receptors BTLA and PD-1. *Cancer Res.* **72,** 887–896 (2012).
26. Crespo, J., Sun, H., Welling, T. H., Tian, Z. & Zou, W. T cell anergy, exhaustion, senescence, and stemness in the tumor microenvironment. *Curr. Opin. Immunol.* **25,** 214–221 (2013).

Supplementary Information is available in the online version of the paper.

Acknowledgements The authors thank A. Bruce and J. Murphy for excellent assistance with artwork.

Author Contributions M.Y. was involved in planning and performing *in vivo* experiments, analysing and interpreting data, and writing the manuscript. S.J. analysed and interpreted whole-exome sequencing and RNA sequencing data, generated translated FASTA database, searched for potential neo-epitopes. Q.T.P. and T.K.C. performed mass spectrometric data analysis and peptide validation. P.L. performed the structure prediction of the MHCI–peptide complexes. J.T. performed studies with tumour-bearing mice. S.B. performed and analysed FACS studies on tumour lines. C.F. performed and analysed immunizations experiments. Z.M. oversaw RNA sequencing experiments. I.M. assisted with the study design and the preparation of the manuscript. J.F. and T.W. performed MHCI peptide isolation and mass spectrometric analysis. L.D and J.R.L. oversaw all the work performed, planned experiments, interpreted data and wrote the manuscript.

Author Information Reprints and permissions information is available at www.nature.com/reprints. The authors declare competing financial interests: details are available in the online version of the paper. Readers are welcome to comment on the online version of the paper. Correspondence and requests for materials should be addressed to L.D. (delamarre.lelia@gene.com) or J.R.L. (lill.jennie@gene.com).

METHODS

MHCI peptide isolation and mass spectrometric analysis. MHCI peptide profiling was conducted for the H-2K^b and H-2D^b 'ligandome' of two murine cell lines of *H-2*^{b}-background: TRAMP-C1 (ATCC) and MC-38 (Academisch Ziekenhuis Leiden) as previously described[27]. Briefly, 1×10^8 cells from each cell line were lysed and MHCI molecules were immunoprecipitated using two different antibodies coupled to CNBr-activated Sepharose resin (GE Healthcare Europe, Freiburg, Germany) in order to extract H-2K^b-specific and H-2D^b-specific peptides, respectively. Antibodies were derived from a local hybridoma culture, H-2K^b-specific antibody from Y3 and H-2D^b-specific antibody from B22.249 clones and purified before use. Peptides were eluted off antibody-resin by acid treatment[27] and purified via ultrafiltration before mass spectrometric analysis.

Peptides were loaded onto an analytical fused-silica micro-capillary column (75 μm internal diameter × 250 mm) packed with 1.7 μm C18 (Waters) and separated by reversed-phase chromatography (nanoAcquity UPLC system, Waters, Milford, MA) using a 180 min gradient. The gradient, composed of Solvent A (0.1% formic acid in water) and Solvent B (0.1% formic acid in acetonitrile) went from 10% to 30% B at a flow rate of 300 nl per minute. The eluted peptides were analysed by data-dependent acquisition (DDA) in an LTQ-Orbitrap Velos hybrid mass spectrometer (Thermo Fisher Scientific, Bremen, Germany) equipped with a nano electrospray ionization source with spray voltage at 2 kV. Mass spectral data was acquired using methods comprising of a full scan (survey scan) of high mass accuracy in the Orbitrap (R = 30,000 for TOP3, R = 60,000 for TOP5), followed by MS/MS (profile) scans either in the Orbitrap (R = 7,500) on the 3 most abundant precursor ions (TOP3) or in the LTQ on the 5 most abundant precursor ions (TOP5) subjected to collision-induced dissociation (CID). Mass range for selection of doubly charged precursors was 400–750 m/z and 800–1,500 m/z for singly charged precursors. Tandem mass spectra data acquisition was triggered for ions of charge state 2 in the TOP5 methods. There were 2 TOP3 methods, one with MS2 triggered for ion charge state 2 and the second method included triggering only singly charged ions. Seven replicate injections were performed for each set of samples.

Synthetic peptides corresponding to identify mutant MC-38 and TRAMP-C1 antigen peptides were analysed on an LTQ-Orbitrap Elite mass spectrometer (ThermoFisher, Bremen, Germany) and ionized using an ADVANCE source (Michrom-Bruker, Fremont, CA) at a spray voltage of 1.2 kV. Peptides were injected onto a 100 μm inner diameter capillary column (NanoAcquity UPLC column, 100 μm × 100 mm, 1.7 μm, BEH130 C18, Waters Corp) and separated by capillary reverse phase chromatography on a NanoAcquity UPLC system (Waters Corp). Samples were loaded in 0.1% formic acid/2% acetonitrile/98%water and eluted with a gradient of 2–90% Buffer B (where Buffer A is 0.1% formic acid/2%acetonitrile/98%water and Buffer B is 0.1% formic acid/ 2% water/ 98% acetonitrile) at 1.00 μl min^{-1} with a total analysis time of 30 min. Mass spectral data were acquired using a method consisting of one full MS scan (375–1,600 m/z) in the Orbitrap at resolution of 60,000 $M/\Delta M$ at m/z 400, followed by MS/MS (profile) scans in the Orbitrap at resolution of 15,000 $M/\Delta M$ at m/z 400 of the peptide ions subjected to collision induced dissociation (CID).

Sequencing. 1 μg of total RNA from MC-38 and TRAMP-C1 cancer cell lines was used to generate RNA-seq libraries using TruSeq RNA sample preparation kit (Illumina, CA). Total RNA was purified from cell lines and fragmented to 200–300 bp, with an average length of 260 bp. RNA-seq libraries were multiplexed (two per lane) and sequenced on HiSeq 2000 as per manufacturer's recommendation (Illumina, CA). 96.1 million (M) RNA fragments were sequenced from MC-38 and 67.5 M from TRAMP-C1. Exome capture was performed using the SureSelectXT mouse exon kit (Agilent, CA). Exome capture libraries were then sequenced on a HiSeq 2000 (Illumina, CA) using the HiSeq sequencing Kit (200 cycles). 60 M (2 × 75 bp) exome reads were sequenced from each cell line.

Read mapping. Reads were mapped to the mouse genome (NCBI build 37 or mm9) using GSNAP[28]. Only uniquely mapped reads were retained for further analysis. 76 M RNA fragments were uniquely mapped in the MC-38 sample and 54.6 M in the TRAMP-C1 sample. 50.9 M exome fragments in MC-38 and 52 M fragments in TRAMP-C1 were uniquely mapped. To obtain mouse gene models, Refseq mouse genes were mapped to the mm9 genome using GMAP[29] and the genomic sequence was then used for making the gene models. Out of a total of 49.6 M targeted by the exome capture, 49 M fragments were covered by uniquely mapped reads in each cell line. Of these, 97.6% were covered by at least 10 reads in MC-38 (97.1% in TRAMP-C1), and 91.7% were covered by at least 20 reads in MC-38, and 91.2% in TRAMP-C1.

Variant calling. Exome-seq based variants were called using GATK[30]. Variants were annotated for effects on transcripts using the variant effector predictor tool[31]. Thus 4,285 coding variants were identified in MC-38 and 949 in TRAMP-C1 (Fig. 1b). RNA-seq based variants from the reference mouse genome were called using these criteria: variant allele should be supported by at least 2 reads, variant allele frequency was greater than or equal to 4%, and variant allele was not strand-biased (based on read alignment to the genome, Fisher's exact test, $P < 0.05$). A vast majority of the variants were supported by exactly 2 reads and these accounted for a majority of variants below 20% variant allele frequency. As an *ad hoc* filter, RNA-seq variants with exactly 2-read support or less than 20% variant allele frequency were filtered out. After overlapping these variants with the exome-based variants, we obtained 1,290 coding variants in MC-38 and 67 such variants in TRAMP-C1 (Fig. 1b).

Reference database for LC-MS (liquid chromatography-mass spectrometry). For each amino acid variation, a variant whole protein sequence was generated to form a set of putative proteins to serve as a reference database for searching LC-MS spectra. In the absence of haplotype information, multiple variations in the same protein would feature as separate variant proteins in the database. The current database was generated without taking into account any haplotype information.

Mass spectrometric data analysis. Tandem mass spectral results were submitted for protein database searching using the Mascot algorithm ver 2.3.02 (MatrixScience, London, UK) against a concatenated target decoy database Uniprot ver 2011_12 or a transcriptome generated FASTA database; comprising of murine proteins and common laboratory contaminants such as trypsin. The data was searched with no enzyme specificity, methionine oxidation (+15.995 Da), and 20 p.p.m. precursor ion mass tolerance. Fragment ion mass tolerance was specified at 0.8 Da or 0.05 Da for MS/MS data acquired in the LTQ or Orbitrap, respectively. Search results were filtered using a linear discriminant algorithm (LDA) to an estimated peptide false discovery rate (FDR) of 5%. The data was further filtered by peptide length, 8–11 amino acids. For the mutated peptide synthetic peptides were generated to validate the sequences.

Modelling of mutant peptide–MHCI complexes. For generation of initial models, peptide–MHC complex structures were chosen from the PDB based on sequence similarity between the mutant peptide and peptide in the model structure. For each mutant peptide model, the following PDB code was used: Reps1, 2ZOL[32]; Adpgk, 1HOC[33]; Dpagt1, 3P9L[34]; Cpne1, 1JUF[35]; Irgq, 1FFN[36]; Aatf, 1BZ9[37]. The Med12 peptide was not modelled due to a lack of a published H-2K^b crystal structure in complex with 10-mer peptide that could be used as a reasonable starting model. The peptide was then modified to the mutant form using COOT[38]. These initial models were then optimized using the Rosetta FlexPepDock web server[19], and the top scoring model chosen for display. The top scoring FlexPepDock models for each peptide were also inspected, and backbone positioning was found to be similar for the top ten models generated. Peptide–MHC images were generated using PyMOL (Schrödinger, LLC).

Immunization of mice with mutated peptides. Research involving animals complied with protocols approved by the Genentech Institutional Animal Care and Use Committee. Age-matched 6–8 weeks old female C57BL/6 mice (The Jackson Laboratory) were injected intraperitoneally with 50 μg long peptide each in combination with adjuvant (50 μg anti-CD40 Ab *clone FJK45* plus 100 μg poly(I:C) (InvivoGen)) in PBS. Mice were immunized on day 0 and day 14 and one week following the last injection, either blood or splenocytes were used for detection of Ag-specific CD8 T cells. To identify peptide-specific T cells, cells were stained with PE-conjugated peptide–MHCI dextramers (MHCI–peptide complex; Immudex, Denmark) for 20 min followed by staining with cell surface markers CD3 (catalogue no. 560527), CD4 (catalogue no. 552775), B220 (catalogue no.552772) (BD Biosciences) and CD8 (catalogue no. 100725, Biolegend). Peptide sequences were as follows Reps1: GRVLELFRAAQLANDVVLQIMELCGATR; Adpgk: GIPVHLELASMTNMEL MSSIVHQQVFPT; Dpagt1: EAGQSLVISASIIVFNLLELEGDYR; Aatf: SKLLSFM APIDHTTMSDDARTELFRS; Irgq: KARDETAALLNSAVLGAAPLFVPPAD; Cpne1: DFTGSNGDPSSPYSLHYLSPTGVNEY; Med12: GPQEKQQRVELSSISN FQAVSELLTFE.

Tumour-infiltrating lymphocytes. Age-matched 6–8 weeks old female C57BL/6 mice were implanted subcutaneously on the right flank with 1×10^5 MC-38 tumour cells. The whole tumour was isolated and digested with collagenase and DNase to isolate TILs. TILs were stained with peptide–MHCI dextramers (as described above) followed by antibodies against CD45 (catalogue no. 561487), CD4 (catalogue no. 553051), CD8 (catalogue no. 553034) (BD Biosciences), Thy1.2 (catalogue no. 140316, BioLegend), PD-1 (catalogue no. 11-9985-82, eBiosciences) and TIM-3 (catalogue no. FAB1529A, R&D Systems). Live/dead stain was used to gate on live cells.

Immunization of tumour-bearing mice. Age-matched 6–8 weeks old female C57BL/6 mice animals were inoculated subcutaneously (right hind flank) with 1×10^5 MC-38 cells in a suspension of Hanks' balanced salt solution (HBSS) and phenol red-free Matrigel (Becton Dickinson Bioscience, San Jose, CA). For prophylactic studies (in Fig. 4a–c) mice were immunized with adjuvant (50 μg anti-CD40 plus 100 μg poly(I:C) or adjuvant with 50 μg Reps1, Adpgk and Dpagt1 peptide each, 3 weeks before the tumour inoculation followed by a boost immunization 2 weeks later. Induction of peptide-specific CD8 T cells was measured in blood a day before inoculation with tumour cells. For vaccination in tumour bearing mice (Fig. 4d–i), C57BL/6 mice were inoculated with 1×10^5 MC-38 tumour cells and 10 days after inoculation (only tumour with volume of approximately 100–150 mm^3 at day 10

were included in the study and were randomly distributed in different groups) mice were injected with adjuvant (anti-CD40 plus poly(I:C)) or adjuvant with 50 μg Reps1, Adpgk and Dpagt1 peptides each. Five mice were randomly chosen for analysis by flow cytometry at day 7 post immunization. One mouse with no tumour in Adj+Pep group did not yield TILs. For tumour study in Fig. 4j, 30 μg anti-CD40 plus 10 μg poly(I:C) of adjuvant dose with 50 μg Reps1, Adpgk and Dpagt1 peptides each was used. Blinded tumour measurements and weights were collected twice a week. Animals exhibiting weight loss of more than 15% of their initial body weight were weighed daily and euthanized if they lose more than 20% of their initial body weight. Animals that exhibited adverse clinical issues were observed more frequently, up to daily depending on the severity, and euthanized if moribund. Mice were euthanized if tumour volumes exceeded 3,000 mm^3, or after 3 months if tumours did not form. Throughout the entire study, clinical observations of all mice were performed twice a week.

Statistical analysis. Sample sizes were chosen empirically to ensure adequate statistical power and were in the line with accepted standards for the techniques employed in the study. Statistical significance was determined with the un-paired two-tailed Student's *t*-test assuming unequal variance at $P \leq 0.05$ level of significance (or indicated in figure legends).

27. Falk, K., Rotzschke, O., Stevanovic, S., Jung, G. & Rammensee, H. G. Allele-specific motifs revealed by sequencing of self-peptides eluted from MHC molecules. *Nature* **351,** 290–296 (1991).
28. Wu, T. D. & Nacu, S. Fast and SNP-tolerant detection of complex variants and splicing in short reads. *Bioinformatics* **26,** 873–881 (2010).
29. Wu, T. D. & Watanabe, C. K. GMAP: a genomic mapping and alignment program for mRNA and EST sequences. *Bioinformatics* **21,** 1859–1875 (2005).
30. DePristo, M. A. *et al.* A framework for variation discovery and genotyping using next-generation DNA sequencing data. *Nature Genet.* **43,** 491–498 (2011).
31. McLaren, W. *et al.* Deriving the consequences of genomic variants with the Ensembl API and SNP Effect Predictor. *Bioinformatics* **26,** 2069–2070 (2010).
32. Butler, N. S. *et al.* Structural and biological basis of CTL escape in coronavirus-infected mice. *J. Immunol.* **180,** 3926–3937 (2008).
33. Young, A. C., Zhang, W., Sacchettini, J. C. & Nathenson, S. G. The three-dimensional structure of H-2D^b at 2.4 Å resolution: implications for antigen-determinant selection. *Cell* **76,** 39–50 (1994).
34. Denton, A. E. *et al.* Affinity thresholds for naive CD8+ CTL activation by peptides and engineered influenza A viruses. *J. Immunol.* **187,** 5733–5744 (2011).
35. Ostrov, D. A. *et al.* How H13 histocompatibility peptides differing by a single methyl group and lacking conventional MHC binding anchor motifs determine self-nonself discrimination. *J. Immunol.* **168,** 283–289 (2002).
36. Wang, B. *et al.* Peptidic termini play a significant role in TCR recognition. *J. Immunol.* **169,** 3137–3145 (2002).
37. Zhao, R., Loftus, D. J., Appella, E. & Collins, E. J. Structural evidence of T cell xeno-reactivity in the absence of molecular mimicry. *J. Exp. Med.* **189,** 359–370 (1999).
38. Emsley, P. & Cowtan, K. Coot: model-building tools for molecular graphics. *Acta Crystallogr. D Biol. Crystallogr.* **60,** 2126–2132 (2004).

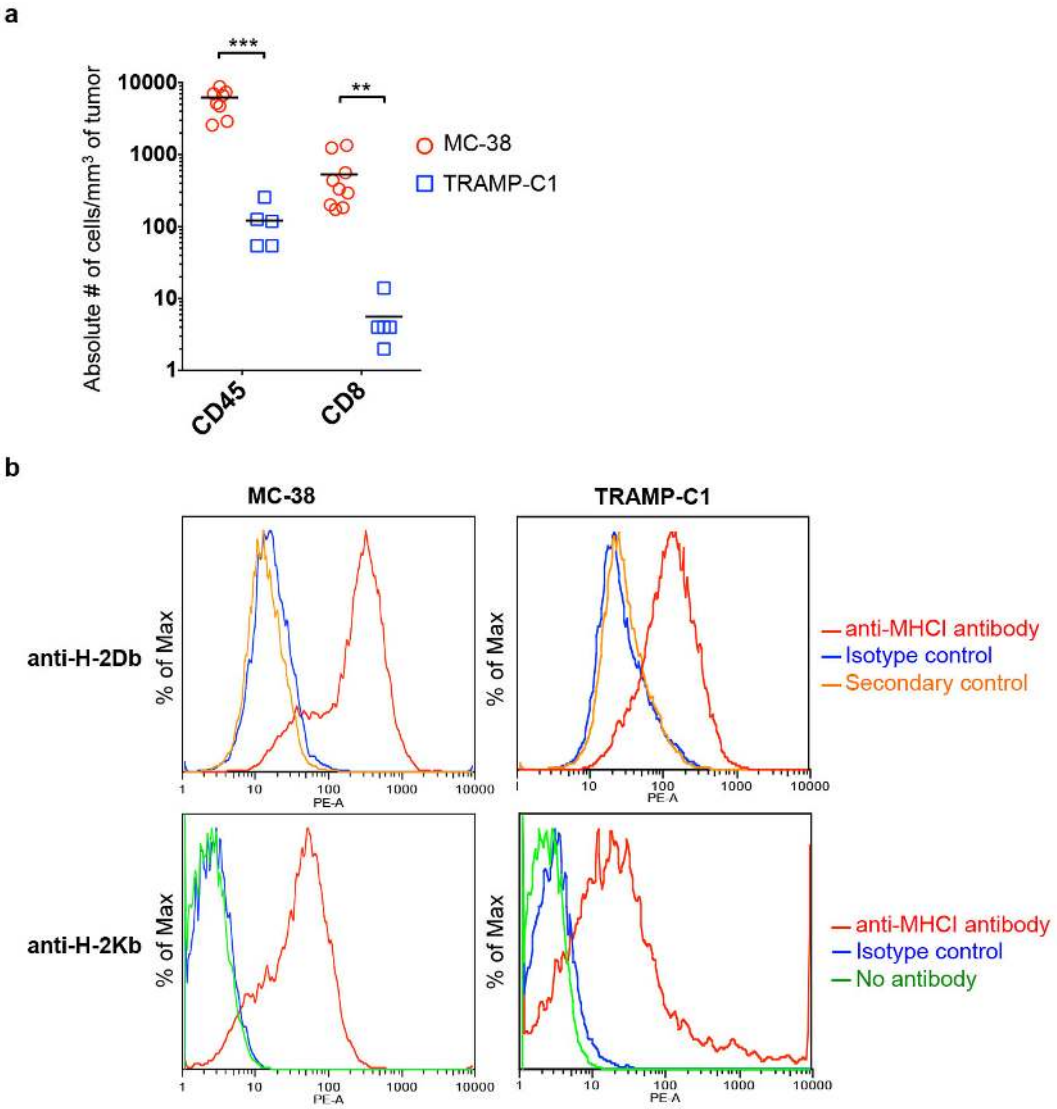

Extended Data Figure 1 | TRAMP-C1 tumours are less immunogenic than MC-38 tumours. **a**, MC-38 or TRAMP-C1 tumours (150–250 mm^3 in size) were grown *in vivo* in C57BL/6 mice. TILs were collected and screened by flow cytometry to quantitate absolute numbers of $CD45^+$ immune cells or CD8 T cells in each tumour sample. $n = 9$ for MC-38 and $n = 5$ for TRAMP-C1. $^{**}P \leq 0.01$, $^{***}P \leq 0.001$ by two-tailed unpaired Student's *t*-test. **b**, MHCI surface expression on MC-38 and TRAMP-C1 cell lines. Cells grown *in vitro* were stained with anti-H-$2D^b$ (biotinylated) or anti-H-$2K^b$ (PE-conjugated) antibodies or isotype controls and analysed for surface expression by flow cytometry.

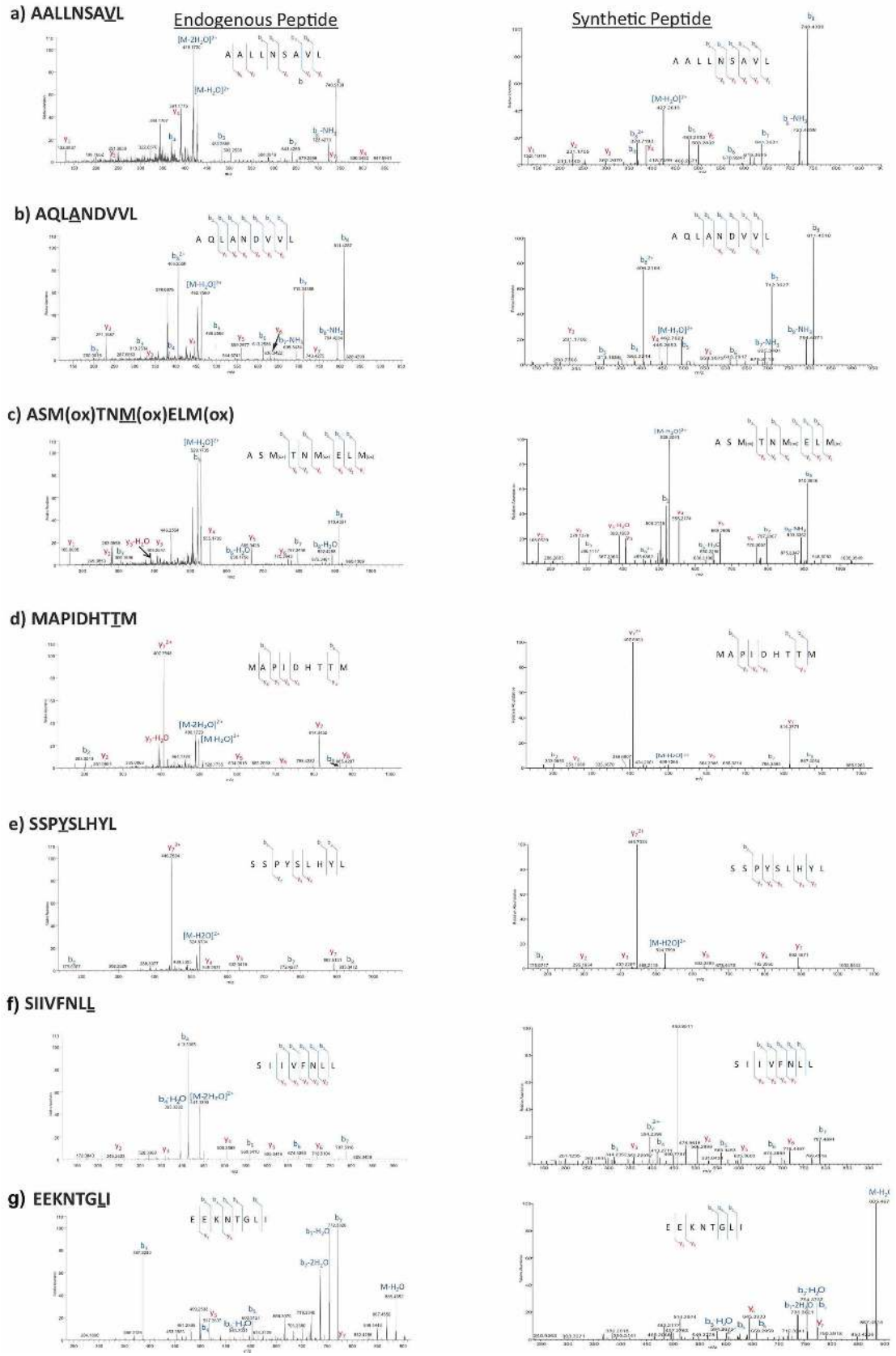

Extended Data Figure 2 | Tandem mass spectra of endogenous mutant MC-38 MHC antigen peptides and their corresponding synthetic peptides. **a**, AALLNSAVL; **b**, AQLANDVVL; **c**, ASM(ox)TNM(ox)ELM(ox), ox, oxidized; **d**, MAPIDHTTM; **e**, SSPYSLHYL; **f**, SIIVFNLL; and **g**, EEKNTGLI. The peak at 460.9511 *m*/*z* corresponds to a co-eluting, singly charged contaminant background ion isolated with peptide precursor (EEKNTGLI is an example of a low-confidence spectral identification, based on comparing the endogenous and synthetic spectra). Mutation sites are indicated with the amino acid underlined. Spectral differences in endogenous and synthetic peptide spectra maybe due to co-eluting peptides in the highly complex sample. Although present, not all fragment ions are labelled due to overlapping peak labels.

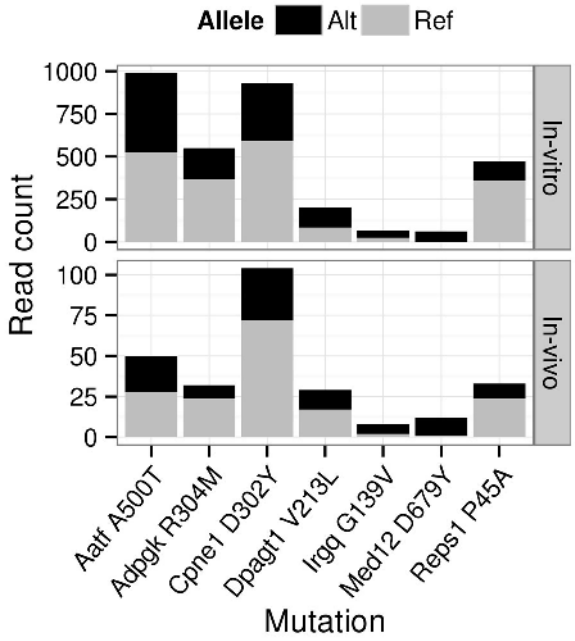

Extended Data Figure 3 | Variant peptide expression is retained *in vivo* for the chosen peptides. Total RNA-seq reads covering the variant position for the genes corresponding to the 7 MS/MS-identified variant peptides are shown. Both the reference and the alternate alleles are shown for an *in vitro* and an *in vivo* sample of the MC-38 line. Expression of the variant allele is observable both *in vitro* and *in vivo*. Alt, alternate allele; Ref, reference allele.

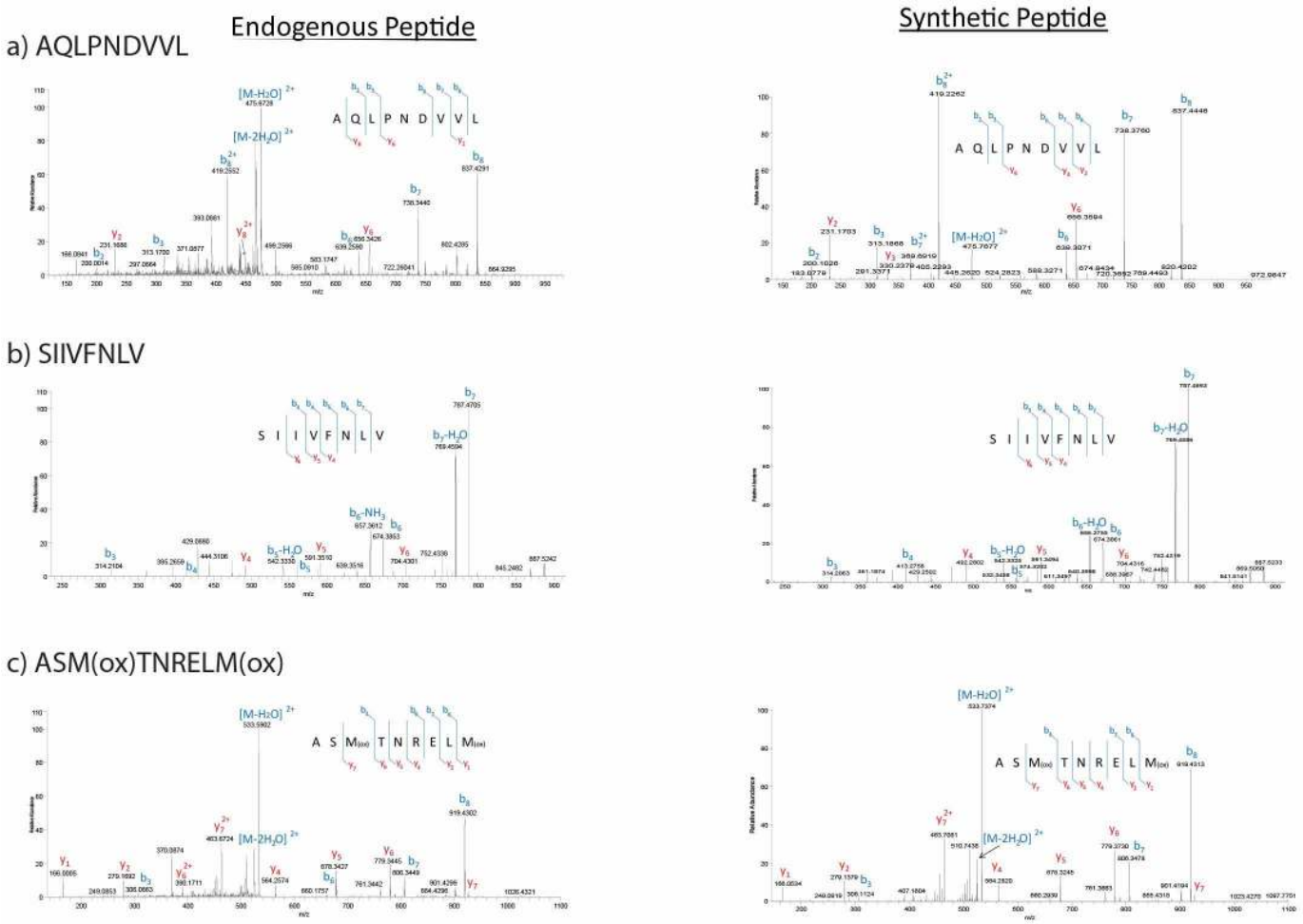

Extended Data Figure 4 | Tandem mass spectra of endogenous wild-type MC-38 MHC antigen peptides and their corresponding synthetic peptides. **a**–**c**, Wild-type MC-38 peptides AQLPNDVVL (**a**), ASM(ox)TNRELM(ox), ox, oxidized **(b)**, and SSISNFQAV **(c)**. Spectral differences in endogenous and synthetic peptide spectra maybe due to co-eluting peptides in the highly complex sample. Although present, not all fragment ions are labelled due to overlapping peak labels.

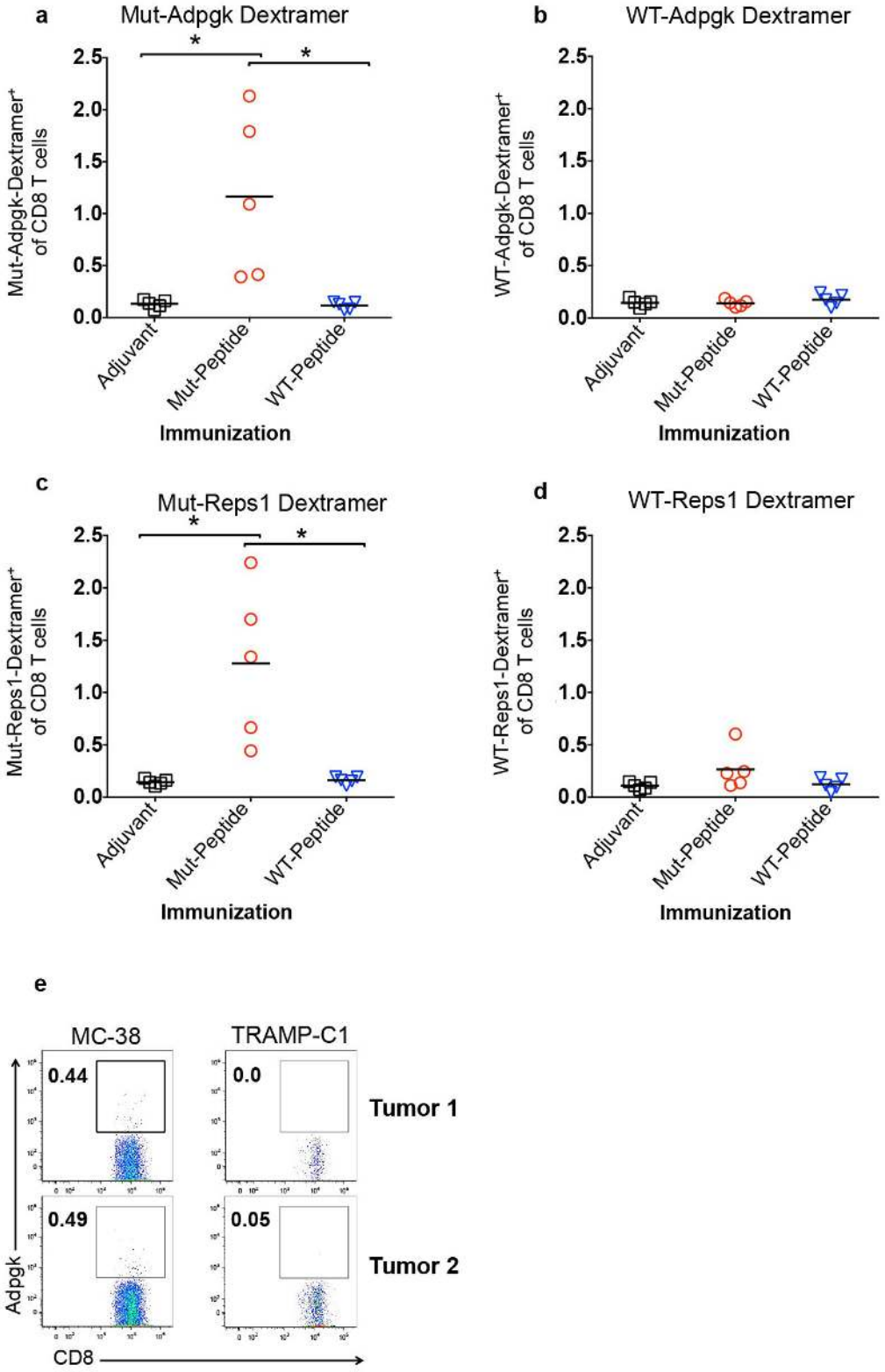

Extended Data Figure 5 | wild-type-counterpart peptides for Adpgk and Reps1 are not immunogenic *in vivo*. **a**–**d**, C57BL/6 mice were immunized with 100 μg wild-type or mutant Adpgk or Reps1 peptides with adjuvant (100 μg Poly (I:C) plus 50 μg anti-CD40) or adjuvant alone, at day 0 and day 14. At day 21, splenic CD8 T cells from mice immunized with wild-type (GIPVHLELASMTNRELMSSIVHQQVFPT) or mutant (GIPVHLELASMTNMELMSSIVHQQVFPT) Adpgk peptide were stained with mut-Adpgk–H-2D^b dextramers (**a**) or WT-Adpgk–H-2D^b dextramers (**b**). Similarly CD8 T cells from mice immunized with wild-type (GRVLELFRAAQLPNDVVLQIMELCGATR) or mutant Reps1 (GRVLELFRAAQLANDVVLQIMELCGATR) peptide were stained with Mut-Reps1/H-2D^b dextramers (**c**) or WT-Reps1/H-2D^b dextramers (**d**) and analysed by flow cytometry. Frequency of indicated peptide–MHCI dextramer$^+$ of CD8 T cells is shown. Mice immunized with adjuvant alone were used as the reference. Data are from one experiment with $n = 5$ each group with bars representing means. *$P \leq 0.05$ (unpaired two-tailed Student's *t*-test). **e**, CD8 TILs from MC-38 or TRAMP-C1 tumours (300–500 mm^3) grown *in vivo* in C57BL/6 mice were stained with PE-labelled Adpgk–H-2D^b dextramers and analysed using flow cytometry. Frequency of Adpgk dextramer$^+$ among CD8 T cells is shown in two different tumour samples.

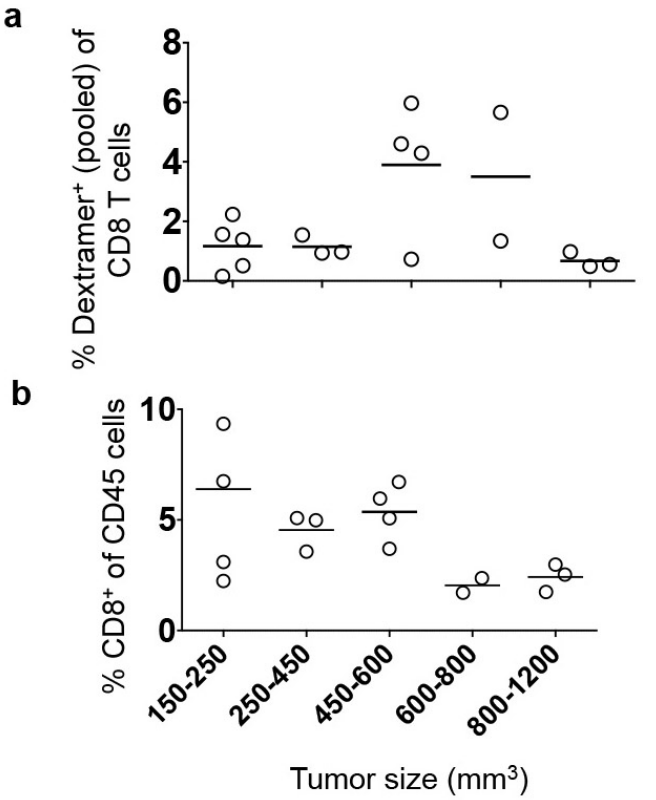

Extended Data Figure 6 | Frequency of peptide-specific CD8 T cells in MC-38 tumours of varying size grown *in vivo* in C57BL/6 mice. **a**, **b**, CD8 T cells in TILs from tumours of indicated sizes were stained with PE-labelled pooled peptide–MHCI dextramers (Adpgk+Reps1+Dpagt1) and analysed by flow cytometry. The graphs are showing percent of peptide–MHCI dextramer$^+$ among CD8 T cells (**a**) and the frequency of CD8 T cells among CD45$^+$ cells (**b**) in TILs. Each point represents an individual mouse and the bars represent means.

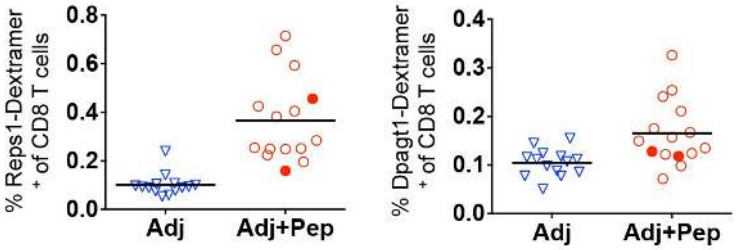

Extended Data Figure 7 | Frequency of Reps1- and Dpagt1-specific CD8 T cells in blood after immunization with peptides. Blood CD8 T cells from C57BL/6 mice were analysed a day before inoculation (at day −1) with MC-38 tumours, after immunization with vaccine as outlined in Fig. 4a. The frequencies of peptide-specific CD8 T cells in the adjuvant alone (Adj) or adjuvant plus peptides (Adj+Pep) groups are shown by staining CD8 T cells with indicated peptide–MHCI dextramers and analysed using flow cytometry. The two mice that developed tumours in Adj+Pep group (in Fig. 4b) are highlighted in red filled circles. Pooled data from two experiments are shown with the bars representing means.

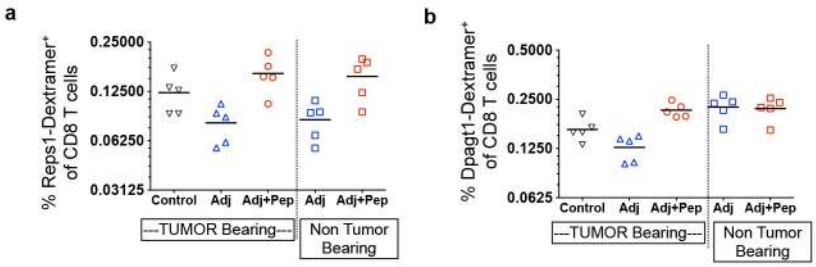

Extended Data Figure 8 | Frequency of Reps1 and Dpagt1-specific CD8 T cells in spleen after immunization of MC-38 tumour bearing or non-tumour-bearing mice. Tumour bearing or non-tumour-bearing C57BL/6 mice were immunized with adjuvant (anti-CD40 plus poly(I:C) alone (Adj) or 50 μg of Reps1, Dpagt1 and Adpgk peptides with adjuvant (Adj+Pep)) as outlined in Fig. 4d. **a**, **b**, Seven days after immunization splenic CD8 T cells were analysed for peptide-specific CD8 T cells by staining with Reps1–H2-Db-specific (**a**) or Dpagt1–H2-Kb-specific (**b**) dextramers and analysed using flow cytometry. Two groups of non-tumour-bearing mice were also immunized and splenic CD8 T cells were analysed at day 7 after immunization. Data are representative of two independent experiments and bars represent means.

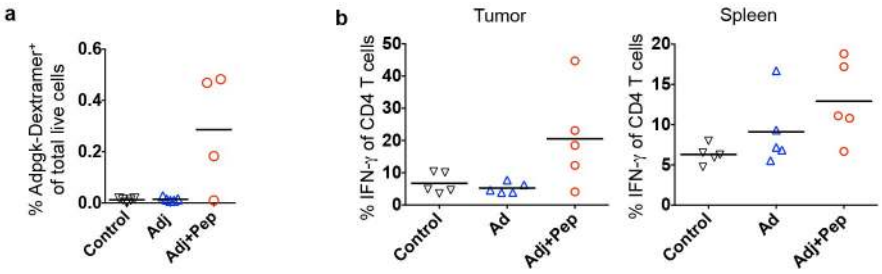

Extended Data Figure 9 | Increased frequency of Adpgk-specific CD8 T cells and IFN-γ-producing CD4 T cells upon immunization of MC-38 tumour-bearing mice. a, Frequency of Adpgk–H-2D^{b} dextramer^{+} CD8 T cells among total live cells in MC-38 tumours. TILs were analysed after immunization of MC-38 tumour bearing C57BL/6 mice with adjuvant alone (Adj) or adjuvant with peptides (Adj+Pep) or no treatment (Control) (as in Fig. 4d). Tumour CD8 T cells were stained with PE-labelled Adpgk–H-2D^{b} dextramers and analysed using flow cytometry. Frequency of Adpgk–H-2D^{b} dextramer^{+} CD8 T cells of total live cells in tumours is shown. **b**, Frequency of IFN-γ expressing CD4 T cells in tumours or spleen at day 7-post immunization. As in Fig. 4i, TILs or splenocytes were stimulated with PMA and ionomycin and IFNγ production among CD4 T cells was determined by intracellular cytokine staining. Data are representative of two independent experiments with bars representing means.